



The fate of an old Mn–Fe amphibole species: description of clino-ferro-suenoite, $\square\text{Mn}_2\text{Fe}_5^{2+}\text{Si}_8\text{O}_{22}(\text{OH})_2$

Dan Holtstam¹, Fernando Cámara², Henrik Skogby¹, Andreas Karlsson¹, and Alessandro De Leo²

¹Department of Geosciences, Swedish Museum of Natural History, Box 50007, 104 05, Stockholm, Sweden

²Dipartimento di Scienze della Terra “A. Desio”, Università degli Studi di Milano,
Via Luigi Mangiagalli 34, 20133, Milan, Italy

Correspondence: Dan Holtstam (dan.holtstam@nrm.se)

Received: 20 November 2024 – Revised: 20 January 2025 – Accepted: 27 January 2025 – Published: 26 March 2025

Abstract. Clino-ferro-suenoite, with the ideal formula $\square\text{Mn}_2\text{Fe}_5^{2+}\text{Si}_8\text{O}_{22}(\text{OH})_2$, previously named “dannemorite” or “manganogrünerite”, is formally recognized as a monoclinic member of the amphibole supergroup (IMA-CNMNC 2024-032). It occurs in iron–manganese skarn from the Hilläng mines, Dalarna, Sweden, associated with fayalite, spessartine, ferro-actinolite, calcite, magnetite and pyrite. It formed by partial replacement of manganiferous fayalite during retrograde metamorphism. Individual crystals, up to 0.5 mm in length, are subhedral with a pale greenish-yellow colour. The mineral is non-pleochroic and optically biaxial (–), with $\alpha = 1.670(5)$, $\beta = 1.690(5)$ and $\gamma = 1.705(5)$; orientation is $y||b$, $z \wedge c = 14(1)^\circ$. Cleavage parallel to $\{110\}$ and $\{010\}$ is perfect and good, respectively. The Mohs hardness is about 6, and the mean Vickers hardness number was established as 872. The calculated density value is $3.46(1) \text{ g cm}^{-3}$. The crystal chemical formula of clino-ferro-suenoite is $^A\square^B(\text{Mn}_{0.95}^{2+}\text{Fe}_{0.87}^{2+}\text{Ca}_{0.16}\text{Na}_{0.01})_{\Sigma 1.99}^C(\text{Fe}_{3.57}^{2+}\text{Mg}_{1.38}\text{Mn}_{0.03}^{2+}\text{Zn}_{0.01}\text{Al}_{0.01})_{\Sigma 5.00}^T\text{Si}_{8.00}\text{O}_{22}^W[(\text{OH})_{1.99}\text{F}_{0.01}]_{\Sigma 2.00}$, based on microprobe analyses, spectroscopic data (Mössbauer, infrared, Raman) and a single-crystal X-ray diffraction study. Infrared bands originating from O–H vibration modes appear at 3608, 3620, 3638, 3653 and 3668 cm^{-1} , with the first and last ones having weak intensities. The seven strongest reflections in the X-ray powder pattern (d values (in Å), I_{rel} , (hkl)) are the following: 8.33, 100, (110); 3.278, 21, (240); 3.084, 72, (310); 2.784, 18, (330); 2.512, 19, (20 $\bar{2}$); 1.526, 16, (0,12,0); 1.412, 19, (66 $\bar{1}$). Unit-cell parameters obtained from single-crystal diffraction data (Mo $K\alpha$) are $a = 9.59840(10)$, $b = 18.3179(2)$, $c = 5.33450(10)$ Å, $\beta = 102.1630(10)^\circ$ and $V = 916.87(2)$ Å³ for $Z = 2$. Refinement of the crystal structure in the space group $C2/m$ yielded $R = 2.25\%$ for 1379 reflections with $I_0 > 2\sigma(I)$. Mg ions show a preference for the octahedrally coordinated C sites in the order $M(2) > M(1) > M(3)$.

1 Introduction

At the time when Häuy (1801) had coined the term “amphibole”, it covered only a handful of the many species of the supergroup recognized today. The number steadily grew during the 50 years thereafter, but there was no member known to carry essential Mn until Erdmann (1851) reported an asbestiform species (denoted “gallbräcka”) from the Dannemora iron mine, Uppland, Sweden, with 8.46 wt % MnO. It was thereafter named “Dannemorit” by Kennigott (1856), soon anglicized to “dannemorite” (Dana, 1857). Notably, the discovery was done at a time before amphiboles

were recognized to contain more than traces of hydrogen (or halogens) and certainly long before the general structural formula $\text{AB}_2\text{C}_5\text{T}_8\text{O}_{22}\text{W}_2$ was established (Cipriani, 2007). The end-member composition $\text{Mn}_2\text{Fe}_5\text{Si}_8\text{O}_{22}(\text{OH})_2$ was not formalized until the first nomenclature scheme emerged, developed by the IMA Subcommittee on Amphiboles (Leake, 1978). “Dannemorite” as a name was then sacrificed in a following nomenclature revision (Leake et al., 1997) in favour of “manganogrünerite”, which was in turn abolished by Hawthorne et al. (2012). According to the present guidelines, a monoclinic $\square\text{Mn}_2\text{Fe}_5\text{Si}_8\text{O}_{22}(\text{OH})_2$ amphibole will be named ferro-clino-suenoite, from its relation

to suenoite (IMA 2019-075) and clino-suenoite (Oberti et al., 2018), which are orthorhombic and monoclinic forms, respectively, of $\square\text{Mn}_2\text{Mg}_5\text{Si}_8\text{O}_{22}(\text{OH})_2$ (equivalent to “root name 3” of Hawthorne et al., 2012). Here we present the complete formal description of the species clino-ferro-suenoite, recently approved by the IMA-CNMNC (no. 2024-032; recommended symbol: Cfsue) and a new member of the magnesium–iron–manganese subgroup.

2 Occurrence

Igelström (1884) described a new mineral species from the Hilläng iron mines, Dalarna, Sweden, under the name “hillängsite” that has been considered synonymous with “dannemorite” (Clark, 1993). A sample of this amphibole from the collections of the Swedish Museum of Natural History was investigated (GEO-NRM no. 19191754) and is now the designated type specimen for clino-ferro-suenoite.

The Hilläng deposit (60°8'49" N, 15°13'10" E; 170 m above the shore line) is situated 1 km east of Ludvika town. The mines, reaching a depth of 370 m, have been worked intermittently over the period 1858–1950. Ore grade was up to 38 % Fe and 12 % Mn, and the total production of lump ore was nearly 1 Mt (Ohlsson, 1979). The ore bodies are located in the western limb of the N–S trending, steeply dipping Stollberg syncline, known to host numerous Fe oxide and Pb–Zn–(Ag) sulfide deposits (e.g., Jansson et al., 2013). Geijer and Magnusson (1944) identified seven different Fe ore types in the Grangärde–Ludvika area, which is dominated by Palaeoproterozoic (1.9–1.8 Ga) granites–granodiorites and metavolcanic and metasedimentary rocks. Hilläng belongs to the category “manganese-rich skarn iron ores”. They are magnetite ore lenses associated with characteristic skarns, mainly Mn-bearing olivine and amphibole. Sulfide mineralization, with galena, sphalerite and arsenopyrite, is also present, locally in high abundance. The host rock to the deposit is a layered, K-enriched rhyolitic metavolcanic unit with skarn bands and marble. The metamorphic grade of the rocks in the area is in the amphibolite facies ($T \leq 600^\circ\text{C}$, $P \sim 3$ kbar; Beetsma, 1992; Ripa, 1994).

Clino-ferro-suenoite occurs with olivine (fayalite–tephroite, $\sim\text{Fa}_{0.70}$) in a dense skarn (Figs. 1 and 2). Associated minerals are garnet (spessartine–almandine), and minor magnetite, pyrite and calcite. A submicroscopic, epitaxially intergrown phase of ferro-actinolite composition occurs sparsely in the main amphibole.

3 Physical and optical description

Clino-ferro-suenoite forms subhedral, short prismatic crystals along [001] that are striated parallel to [001] and up to 0.5 mm in length. The colour is pale greenish-yellow to colourless, with a white streak. The crystals are vitreous, transparent, without fluorescence effects shown under UV



Figure 1. Colour image of skarn assemblage with a clino-ferro-suenoite aggregate in the centre. Darker areas are olivine. Sample GEO-NRM no. 19191754.

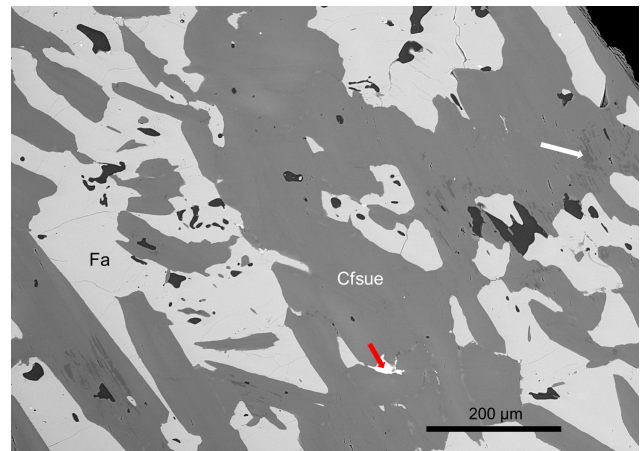


Figure 2. Backscattered-electron scanning electron microscopy (BSE-SEM) image of a polished section of clino-ferro-suenoite (Cfsue) with olivine (Fa). Darkest grains are calcite. The red arrow points to magnetite. Dark grey zones in the amphibole crystals are close to ferro-actinolite (white arrow). Sample GEO-NRM no. 19191754.

light. Mohs hardness is ~ 6 ; from micro-indentation measurements (Vickers) with a 100 g weight under 15 s, a mean value of 872 (range 748–1075 from 10 measurements) is obtained. The amphibole is brittle with an uneven, splintery fracture and shows {110} perfect and {010} imperfect cleavages. Density could not be measured because of its intergrown character and a value expected to be higher than available liquids; a number calculated from unit-cell volume and chemical data (see below) is $3.46(1) \text{ g cm}^{-3}$. Clino-ferro-suenoite is optically biaxial (–) and non-pleochroic, with $\alpha = 1.670(5)$, $\beta = 1.690(5)$ and $\gamma = 1.705(5)$ in white light. $2V$ is estimated at $80 \pm 10^\circ$, and $2V_{\text{calc}} = 80.9^\circ$.

The compatibility index obtained from Gladstone–Dale constants (Mandarino, 2007) is 0.018 (category: superior).

Table 1. Chemical data (in wt %) for clino-ferro-suenoite based on electron microprobe analyses.

Constituent	Mean	Range	2 σ	Reference material
Na ₂ O	0.02	0.00–0.06	0.02	Omphacite
MgO	5.83	5.54–6.07	0.12	Olivine
Al ₂ O ₃	0.06	0.04–0.11	0.02	Grossular
SiO ₂	50.46	50.16–50.87	0.23	Grossular
K ₂ O	0.01	0.00–0.03	0.01	K-feldspar
CaO	0.91	0.79–1.21	0.12	Grossular
TiO ₂	0.02	0.00–0.06	0.02	Ilmenite
MnO	7.31	7.05–7.55	0.14	Rhodonite
FeO*	33.45	33.19–33.70	0.56	Fayalite
ZnO	0.11	0.00–0.20	0.07	Zinc metal
F	0.02	0.00–0.06	0.02	Fluorapatite
H ₂ O _{calc}	1.89	1.85–1.89	0.01	
Total	100.10			

* Only Fe²⁺ is present, based on Mössbauer spectroscopy.

4 Chemical data

The chemical composition (Table 1) was determined using a JEOL 8200 SuperProbe electron microprobe (wavelength dispersive spectrometry, WDS), working at 15 kV and 5 nA probe current, with a beam size of > 1 μ m. Natural and synthetic reference materials were employed (Table 1). The number of spot analyses was 10. The presence of H₂O was inferred from structural data and vibrational spectroscopy and calculated according to OH + F = 2 atoms per formula unit (apfu). Analyses of subordinate amphibole inclusion and olivine are reported in Table S1. Trace elements were analysed with laser ablation inductively coupled plasma mass spectrometry (LA-ICP-MS, Thermo Fisher Scientific ICP-MS iCAP-RQ single quadrupole, at the Geochemistry, Geochronology and Isotope Geology laboratory, Università di Milano) using basaltic glass reference material GSD-2G (Wilson, 2018) as primary standard. Glass reference materials ARM-3 (Wu et al., 2019) and BCR-2G (Jochum et al., 2005) were analysed as quality control. The results are reported in Table S2. The analysed crystal is displayed in Fig. 3.

The empirical formula of type clino-ferro-suenoite calculated on the basis of 24 (O, OH) is Fe_{4.44}²⁺Mg_{1.38}Mn_{0.98}²⁺Ca_{0.16}Na_{0.01}Zn_{0.01}Al_{0.01}Si_{8.00}O_{23.99}F_{0.01}H_{1.99}, and the assigned crystal chemical formula (see the Discussion section) is $A\Box^B(Mn_{0.95}^{2+}Fe_{0.87}^{2+}Ca_{0.16}Na_{0.01})_{\Sigma 1.99}^C(Fe_{3.57}^{2+}Mg_{1.38}Mn_{0.03}^{2+}Zn_{0.01}Al_{0.01})_{\Sigma 5.00}^T Si_{8.00}O_{22}^W[(OH)_{1.99}F_{0.01}]_{\Sigma 2.00}$. The ideal formula is $\Box Mn_2^+ Fe_5^+ Si_8 O_{22} (OH)_2$, which would require the composition SiO₂ 48.08, FeO 35.93, MnO 14.19, H₂O 1.80 for sum 100.00 wt %.

The amphibole is very low (< 1 ppm) in most of the measured trace elements, including Li, Be, Pb and transition metals, but contains ~ 12 ppm Sc and 50–60 ppm Ti.

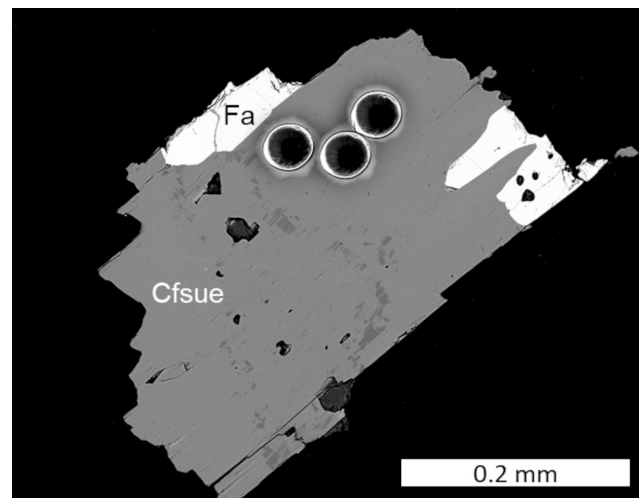


Figure 3. BSE-SEM image of a clino-ferro-suenoite (Cfsue) crystal with fayalite (Fa) analysed by electron microprobe and LA-ICP-MS. The three craters on the upper part of the crystal are from the LA-ICP-MS point analyses.

The chondrite-normalized rare-earth-element (REE) curve (Fig. 4) is downward concave with a positive Eu anomaly.

5 X-ray diffraction data

5.1 Powder

X-ray powder diffraction data (Table 2) were collected with a PANalytical X'Pert³ powder diffractometer equipped with an X'celerator silicon-strip detector and operated at 40 mA and 45 kV (Cu K α radiation, $\lambda = 1.5406 \text{ \AA}$). The monoclinic unit-cell parameters refined from the powder data, using least-squares fitting with minimization on $Q = 1/d^2$ (Hol-

Table 2. X-ray powder diffraction data (d in Å) for clino-ferro-suenoite.

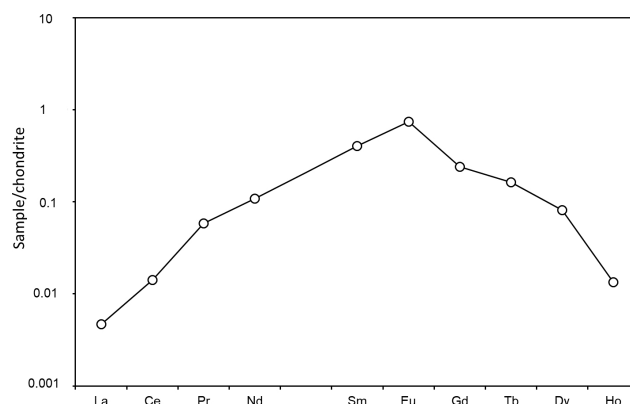
I (obs.)	I (calc.)	d (obs.)	d (calc.)	h	k	l
8	16	9.13	9.1655	0	2	0
100	100	8.33	8.3533	1	1	0
9	6	4.688	4.6921	2	0	0
6	7	4.578	4.5828	0	4	0
15	7	4.173	4.1766	2	2	0
3	22	3.459	3.4536	1	3	1
21	21	3.278	3.2785	2	4	0
72	46	3.084	3.0835	3	1	0
5	14	2.995	2.9910	2	2	1
18	7	2.784	2.7844	3	3	0
15	58	2.762	2.7581	1	5	1
13	30	2.6361	2.6345	0	6	$\bar{1}$
26	19	2.5121	2.5141	2	0	$\bar{2}$
7	1	2.4212	2.4253	2	2	$\bar{1}$
8	16	2.3109	2.3107	3	5	$\bar{1}$
11	26	2.2009	2.1979	2	6	1
3	13	2.0861	2.0932	2	0	2
5	9	2.0447	2.0421	3	5	1
3	7	1.9639	1.9632	4	0	$\bar{2}$
2	1	1.8847	1.8878	1	9	$\bar{1}$
6	3	1.6866	1.6868	5	5	$\bar{1}$
12	18	1.6660	1.6649	4	6	1
10	8	1.6395	1.6408	1	11	0
3	13	1.5983	1.5971	1	5	$\bar{3}$
9	4	1.5637	1.5640	6	0	0
16	4	1.5262	1.5276	0	12	0
6	3	1.4699	1.4689	1	7	$\bar{3}$
19	8	1.4125	1.4137	6	6	$\bar{1}$

land and Redfern, 1997), are the following: $a = 9.6060(9)$ Å, $b = 18.3310(17)$ Å, $c = 5.3252(6)$ Å, $\beta = 102.335(11)^\circ$ and $V = 916.05(12)$ Å³ for $Z = 2$.

5.2 Single crystal

A single-crystal X-ray study was done on an $254 \times 102 \times 56$ µm fragment using a Rigaku Oxford Diffraction XtaLAB Synergy diffractometer, equipped with a PhotonJet (Mo) X-ray source operating at 50 kV and 1 mA, with a monochromatized Mo $K\alpha$ radiation and equipped with a HyPix detector working at 62 mm from the crystal. A combination of ω scans at different values of ϕ , κ and θ positions, with a step scan of 0.5° and exposure times of 3 and 10 s per frame, was used to maximize redundancy and data coverage.

The crystal structure of clino-ferro-suenoite was refined with SHELXL (Sheldrick, 2015), starting from the atom coordinates of grunerite of Finger (1969). When the $M(4)$ site is refined with isotropic displacement parameters, the observed y/b coordinate for the $M(4)$ of ca. 0.26, closer to the strip of octahedra, which is typical of $B(\text{Fe}^{2+}, \text{Mn}^{2+})$ amphiboles (see, for instance, $C2/m$ cummingtonite by Yang

**Figure 4.** Chondrite-normalized REE pattern for clino-ferro-suenoite, based on LA-ICP-MS analyses.

et al. (1998), reporting a value of 0.2592 at ambient P). With this setting, the first maximum in the Fourier-difference map (with a density $2.5 \text{ e}^- \text{ \AA}^{-3}$) is observed at $(0, 0.286, 0)$, which is usually found for the $M(4)$ site in calcic and sodic amphiboles (a value of $y/b = 0.278$ is reported for tremolite by Merli et al., 2000). The presence of 0.16 apfu Ca in the empirical formula agrees with the possibility of Ca (and Na) ordered at this position. However, a model refining a split site with Ca at the usual y/b coordinate for $M(4)$ site was unstable. Therefore, the $M(4)$ was refined as a single site with anisotropic displacement parameters. With this model, the first maximum in the Fourier-difference map corresponded to the position of the proton bonded to the O(3) site. The coordinates were thus added to the model and refined along with an isotropic displacement parameter. The model converged to $R = 2.25\%$ for 1307 unique reflections.

Crystal and experimental data are summarized in Table 3. Refined atom coordinates, site scattering and equivalent isotropic displacement parameters are reported in Table 4. Selected interatomic distances and bond angles are given in Table 5. Site populations for clino-ferro-suenoite have been derived from the empirical formula and the results of the structure refinement (Table 6; see the Discussion section).

There is an excellent agreement between the refined values of the site scattering and mean bond lengths and those calculated based on the proposed site populations. A crystallographic information file (CIF) containing observed structure factors has been deposited in the Supplement.

The tetrahedrally coordinated T sites are completely filled with Si, whereas the very minor Al is assigned to $M(2)$. The $M(4)$ site (equivalent to the B position) has a mixed occupancy with $\text{Mn} > \text{Fe} \gg \text{Ca} \gg \text{Na}$. The residual electron density at the A site is zero, in agreement with the exceptionally low alkali content (Table 1). From the spectroscopic and chemical data, it is clear that the present specimen is a nearly pure hydroxy-amphibole.

Table 3. Crystal data and structure refinement.

Temperature (K)	298
Crystal system	monoclinic
Space group	<i>C2/m</i>
<i>a</i> (Å)	9.59840(10)
<i>b</i> (Å)	18.3179(2)
<i>c</i> (Å)	5.33450(10)
β (°)	102.1630(10)
Volume (Å ³)	916.87(2)
<i>Z</i>	2
ρ_{calc} (g cm ⁻³)	3.46
μ (mm ⁻¹)	5.227
<i>F</i> (000)	930.0
Crystal size (mm)	0.254 × 0.102 × 0.056
Radiation	Mo <i>K</i> α ($\lambda = 0.71073$)
2 Θ range for data collection (°)	7.816 to 59.962
Index ranges	$-13 \leq h \leq 13, -25 \leq k \leq 25, -7 \leq l \leq 7$
Reflections collected	24470
Independent reflections	1379 ($R_{\text{int}} = 0.0328, R_{\text{sigma}} = 0.0110$)
Data/restraints/parameters	1379/0/102
Goodness-of-fit on <i>F</i> ²	1.140
Final <i>R</i> indexes ($I \geq 2\sigma(I)$)	$R_1 = 0.0225, wR_2 = 0.0692$
Final <i>R</i> indexes (all data)	$R_1 = 0.0236, wR_2 = 0.0699$
Largest diff. peak/hole or e (Å ⁻³)	0.80/−0.53

Table 4. Refined fractional atomic coordinates ($\times 10^4$) and equivalent isotropic displacement parameters (Å² × 10³). *U*_{eq} is defined as 1/3 of the trace of the orthogonalized *U*^{*ij*} tensor. BVS is the bond valence sum (in valence units) calculated with the parameters of Gagné and Hawthorne (2015).

Atom	Occup.*	<i>x</i>	<i>y</i>	<i>z</i>	<i>U</i> _{eq}	BVS
<i>M</i> (1)	Fe 0.869(2)	0	876.9(2)	5000	11.51(14)	2.080
<i>M</i> (2)	Fe 0.800(2)	0	1789.7(2)	0	11.39(15)	2.071
<i>M</i> (3)	Fe 0.872(3)	0	0	0	10.60(18)	2.121
<i>M</i> (4)	Mn 0.996(2)	0	2596.4(2)	5000	15.39(13)	1.900
<i>T</i> (1)	Si 1.00	2858.6(5)	837.3(2)	2726.2(8)	9.91(12)	4.044
<i>T</i> (2)	Si 1.00	2972.0(4)	1676.3(2)	7793.6(7)	10.71(12)	3.971
O(1)	O 1.00	1138.5(13)	878.9(5)	2077(2)	11.6(2)	2.046
O(2)	O 1.00	1248.9(13)	1738.0(6)	7158(2)	12.7(2)	2.019
O(3)	O 1.00	1139.8(18)	0	7062(3)	13.8(3)	1.067
O(4)	O 1.00	3804.2(13)	2431.1(6)	7716(2)	16.0(2)	1.930
O(5)	O 1.00	3487.5(12)	1284.7(6)	589.8(19)	15.4(2)	1.982
O(6)	O 1.00	3481.0(12)	1189.2(7)	5539(2)	17.6(2)	2.023
O(7)	O 1.00	3390.9(17)	0	2735(3)	16.1(3)	2.039
H	H 1.00	2190(50)	0	7460(80)	57(13)	0.845

* Occup. means site scattering fraction.

6 Spectroscopic data

6.1 Raman micro-spectroscopy

A Raman spectrum was obtained at Laboratorio di Mineralogia Sperimentale “Fiorenzo Mazzi”, Università di Pavia, with a LabRAM HR Evol equipped with a Symphony BIDD detector and 532 nm laser. A second spectrum was collected at

the Swedish Museum of Natural History with a LabRAM HR 800 and a 515 nm laser. Measurements at both labs were done with 100× VIS (visible) objectives (600 grooves mm⁻¹ gratings), and the spectra were calibrated against metallic Si. Although showing some variations in relative intensities, peak positions obtained were almost identical between the two experiments (± 2 cm⁻¹).

Table 5. Selected interatomic distances (Å) in clino-ferro-suenoite.

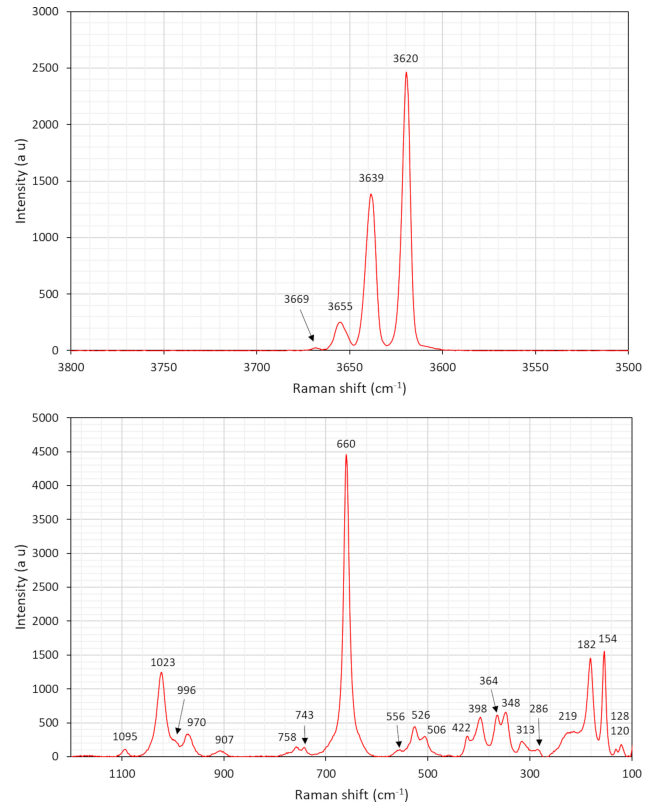
$M(1)-O1$	2.0840(12)	$T(1)-O1$	1.6157(13)
$M(1)-O1^c$	2.0840(12)	$T(1)-O5$	1.6201(11)
$M(1)-O2$	2.1606(11)	$T(1)-O6$	1.6268(11)
$M(1)-O2^c$	2.1606(11)	$T(1)-O7$	1.6164(7)
$M(1)-O3$	2.1166(11)	$\langle T(1)-O \rangle$	1.620
$M(1)-O3^a$	2.1166(11)	Vol (Å ³)	2.18
$\langle M(1)-O \rangle$	2.120	TAV (° ²)	0.72
Vol (Å ³)	12.52	TQE	1.0002
OAV (° ²)	33.38	$T(2)-O2$	1.6207(13)
OQE	1.0104	$T(2)-O4$	1.6016(12)
$M(2)-O1$	2.1669(11)	$T(2)-O5^b$	1.6350(11)
$M(2)-O1^c$	2.1669(11)	$T(2)-O6$	1.6519(11)
$M(2)-O2^c$	2.1240(12)	$\langle T(2)-O \rangle$	1.627
$M(2)-O2^d$	2.1240(12)	Vol (Å ³)	2.20
$M(2)-O4^f$	2.0614(11)	TAV (° ²)	15.99
$M(2)-O4^g$	2.0614(11)	TQE	1.0041
$\langle M(2)-O \rangle$	2.117	$M(4)-O2^c$	2.1572(11)
Vol (Å ³)	12.48	$M(4)-O2$	2.1572(11)
OAV (° ²)	32.40	$M(4)-O4^g$	2.0299(12)
OQE	1.0099	$M(4)-O4^j$	2.0299(12)
$M(3)-O1^e$	2.1222(11)	$M(4)-O6$	2.7081(13)
$M(3)-O1^h$	2.1222(11)	$M(4)-O6$	2.7081(13)
$M(3)-O1^i$	2.1222(11)	$\langle M(4)-O \rangle$	2.298
$M(3)-O1$	2.1222(11)	Vol (Å ³)	11.98
$M(3)-O3^a$	2.0918(17)	OAV (° ²)	437.44
$M(3)-O3^d$	2.0918(17)	OQE	1.2423
$\langle M(3)-O \rangle$	2.112	O3-H	0.99(5)
Vol (Å ³)	12.28	O5-O6-O5	172.49(7)
OAV (° ²)	50.51	O6-O7-O6	111.61(8)
OQE	1.0156	$T(1)-O7-T(1)$	143.21(11)

^a $-x, -y, 1 - z$; ^b $+x, +y, 1 + z$; ^c $-x, +y, 1 - z$; ^d $+x, +y, -1 + z$; ^e $-x, +y, -z$; ^f $-1/2 + x, 1/2 - y, -1 + z$; ^g $1/2 - x, 1/2 - y, 1 - z$; ^h $+x, -y, +z$; ⁱ $-x, -y, -z$; ^j $-1/2 + x, 1/2 - y, +z$; OQE, OAV, TQE and TAV are the octahedral and tetrahedral angle variance and quadratic elongation of Robinson et al. (1971).

The resulting spectra (Figs. 5 and 6) have distinct common features with that of grunerite (Apopei et al., 2011). The multiple bands around 3600–3670 cm⁻¹ are related to OH-stretching vibration modes. A group of bands in the region 900–1100 cm⁻¹ is ascribed to Si–O symmetric and anti-symmetric stretching. Two weak bands at 743 and 758 cm⁻¹ are assigned to $M \cdots O-H$ bending. The intense signal at 660 cm⁻¹ is connected to Si–O–Si bending. The bands situated at 490–560 cm⁻¹ may be assigned to bending modes of Si₄O₁₁ units. The significant peak at 348 cm⁻¹ is tentatively assigned to stretching vibrations of ^CFe²⁺–O octahedra, and the peak at 364 cm⁻¹ is assigned to Mg–O vibrations. Marked bands at 154–215 cm⁻¹ likely represent framework vibrations related to metal–O modes.

6.2 Fourier-transform infrared (FTIR) spectroscopy

Polarized single-crystal FTIR spectra were collected in the range 2000–10 000 cm⁻¹ at a spectral resolution of 1 cm⁻¹

**Figure 5.** Raman spectra of clino-ferro-suenoite obtained with a 532 nm laser.

on a 50 × 100 μm raster, with a Bruker Vertex 70 spectrometer attached to a Bruker Hyperion 2000 IR microscope. Measurements were done from a 43 μm thick doubly polished single-crystal fragment oriented parallel to (010). The spectra in the X direction (Fig. 7) show distinct absorption bands at 3620, 3638, and 3653 cm⁻¹, plus a weak band at 3668 cm⁻¹ and a very weak one at 3608 cm⁻¹, caused by O–H stretching vibrations of the OH dipole at the O(3) position. These bands observed (both in FTIR and Raman spectra) correspond to the local atomic environments $M(1)M(2)M(3)-T-O(3)$ of Fe²⁺Fe²⁺Fe²⁺–Si–OH, Fe²⁺Fe²⁺Mg–Si–OH, Fe²⁺MgMg–Si–OH and Mg–Mg–Mg–Si–OH, respectively (Leißner, 2014). The weakest signal at 3608 cm⁻¹ may be related to the minor amounts of Mn²⁺ disordered over C positions (cf. Hawthorne and Della Ventura, 2007).

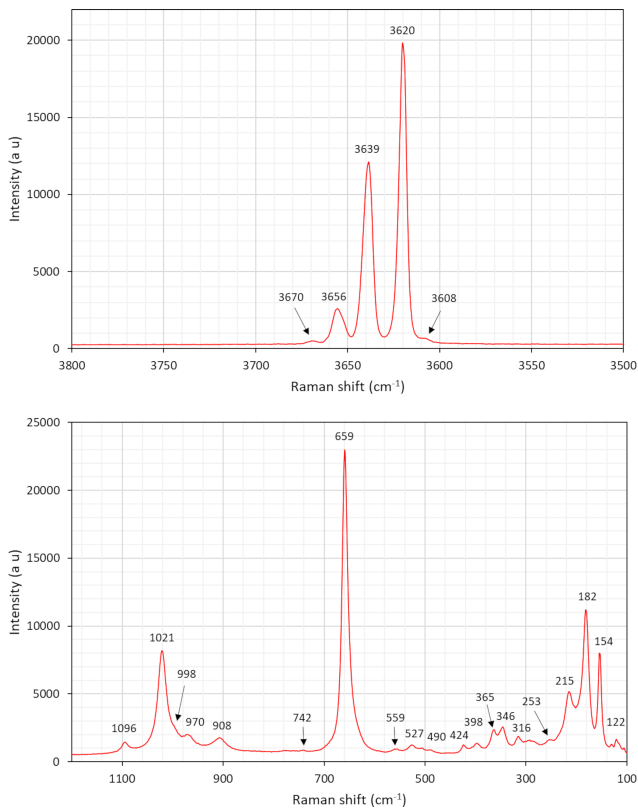
6.3 Mössbauer spectroscopy

Crystal fragments were handpicked under a binocular microscope from a crushed sample and sieved with a 100 μm mesh. The ⁵⁷Fe transmission Mössbauer spectrum (Fig. 8) was obtained from a 10 mg powder absorber (with 100 mg acrylic resin added) using a constant acceleration mode spectrometer (WissEl) and standard ⁵⁷Co γ radiation source in a Rh matrix (nominally 1.8 GBq). Two mirror-image spectra

Table 6. Site populations for clino-ferro-suenoite.

Site	Site population (apfu)	ss (epfu)		mbl (Å)	
		refined	calculated	refined	calculated*
<i>T</i> (1)	4 Si	56.0	56.0	1.620	1.620
<i>T</i> (2)	4 Si	56.0	56.0	1.627	1.629
<i>M</i> (1)	1.51 Fe ²⁺ + 0.47 Mg + 0.01 Mn ²⁺ + 0.01 Zn	45.19(2)	45.45	2.120	2.119
<i>M</i> (2)	1.27 Fe ²⁺ + 0.70 Mg + 0.02 Mn ²⁺ + 0.01 Al	41.6(1)	42.05	2.117	2.117
<i>M</i> (3)	0.79 Fe ²⁺ + 0.21 Mg	22.67(5)	23.06	2.112	2.109
ΣC cations	3.60 Fe ²⁺ + 1.38 Mg + 0.01 Zn + 0.01 Al	109.46	110.56		
B cations	0.95 Mn ²⁺ + 0.87 Fe ²⁺ + 0.16 Ca + 0.01 Na	49.8(1)	49.68		
A cations	0				
W anions	1.99 (OH) + 0.01 F	16	16.02		

* Using the equations of Oberti et al. (2007). ss: site scattering. mbl: mean bond length. epfu: electrons per formula unit. apfu: atoms per formula unit.

**Figure 6.** Raman spectra of clino-ferro-suenoite obtained with a 515 nm laser.

($\pm 4.28 \text{ mm s}^{-1}$) were collected at 54.7° geometry to avoid orientation effects of crystallites, during 3 d over 1024 channels, and calibrated against a $25 \mu\text{m}$ α -iron foil. The baseline of the resulting folded spectrum was at ca. 8.24×10^6 counts. Fitting and analysis were done with the MossA software (Prescher et al., 2012), assuming Lorentzian line shapes and identical recoil-free fractions for all crystallographic sites

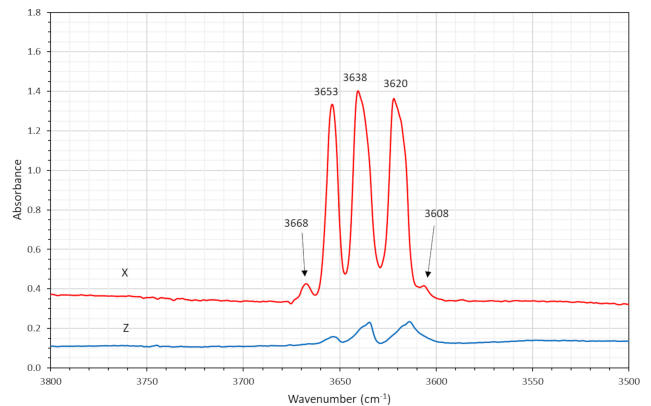
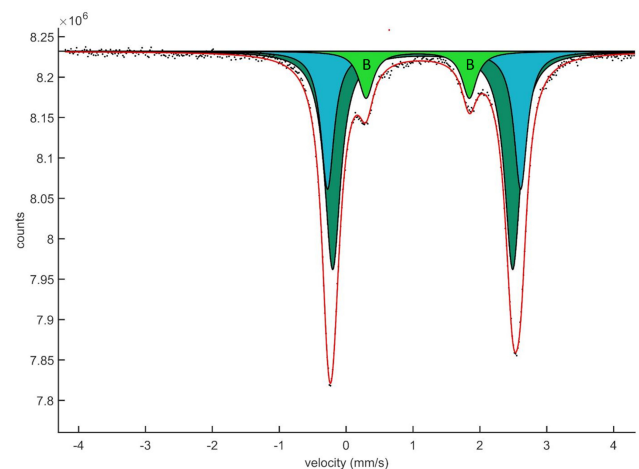
**Figure 7.** Polarized single-crystal FTIR spectra of clino-ferro-suenoite.**Figure 8.** Transmission ⁵⁷Fe Mössbauer spectrum of clino-ferro-suenoite. The inner doublet originates from Fe²⁺ at the B position (*M*4 site).

Table 7. Mössbauer data for clino-ferro-suenoite.

Isomer shift (mm s ⁻¹)	Quadrupole splitting (mm s ⁻¹)	Absorption area (%)	Assignment
1.160(4)	2.86(2)	49(4)	^C Fe ²⁺
1.142(4)	2.65(2)	39(4)	^C Fe ²⁺
1.070(8)	1.55(2)	12(4)	^B Fe ²⁺

Errors given as 2σ.

with Fe atoms. The line width (full width at half maximum) was 0.26(4) mm s⁻¹, and a χ² of 1.5 was achieved for the fitting.

The hyperfine parameters obtained (Table 7) are very similar to those found for grunerite (Zhang and Hafner, 1992). The dominant absorption doublet, ascribed to Fe²⁺ at the octahedrally coordinated cation sites *M*(1-2-3) with a centroid shift (CS) around 1.15 mm s⁻¹, can here be fitted with two line pairs of equal widths, separated by slightly different quadrupole splitting (QS) values. As observed previously for monoclinic magnesium-iron amphiboles (Goldman, 1979; Zhang and Hafner, 1992; Boffa Ballaran et al., 2002), the distribution of Fe²⁺ over the *M*(1-2-3) sites can hardly be accurately determined from Mössbauer spectra because of severe line overlaps and next-nearest-neighbour effects. A model which groups the Fe content of the geometrically similar *M*(1) and *M*(2) sites together and keeps *M*(3) distinct does not give a good match with the fractions obtained from the area ratios of the doublet pairs.

A smaller contribution, ~ 12 % of total absorption, emanating from a doublet at CS = 1.07 mm s⁻¹, is attributed to Fe²⁺ at *M*(4). This assignment is in agreement with a low QS value, 1.55 mm s⁻¹, related to the distorted symmetry of the site, and is quite distinct from the larger values obtained for Fe²⁺ at the more regular *M*(1-2-3) sites (Greenwood and Gibb, 1971). The fraction is less than what would be expected for the crystal chemical formula above, 19.6 %. The discrepancy can be explained by the fact that the absorber is > 1000 times larger than the volume analysed by single-crystal X-ray diffraction and electron microprobe, not being fully representative of the composition of the crystal type and likely also including impurities.

No resonant absorption due to Fe³⁺ could be observed in the Mössbauer spectrum, suggesting that the fraction is almost negligible, < 2 % of total absorption.

7 Discussion

The site assignments reported in Table 6 have been calculated considering several factors: polyhedral sizes, refined site scattering and known site preferences. To calculate the mean bond lengths reported in Table 6, we used the equations reported by Hawthorne and Oberti (2007) in their Table 7. The average ionic radii were calculated using the ionic radii

of Shannon (1976). The preference of Mg for smaller octahedral coordination would place it fully ordered at the *C* sites. The site preference obtained for Mg, *M*(2) > *M*(1) > *M*(3), is in agreement with the arrangement of C cations found in previous studies of grunerite-cumingtonite (e.g., Finger, 1969; Hirschmann et al., 1994; Yong et al., 2019). The scattering power of Mn is very close to Fe; therefore, it is difficult to obtain site partitioning of Mn²⁺ using refined site scattering alone. Following Oberti et al. (1997), the site preference is *M*(4) ≫ *M*(2) ≫ *M*(1) ≫ *M*(3). We have thus considered the stronger preference of Mn²⁺ for larger sites, placing most of this cation at the *B* sites. Only small amounts of Mn²⁺ have been located at the *M*(1) and *M*(2) sites to obtain the best agreement among the observed and calculated < *M*(1-2-3)-O > distances. The best compromise among calculated site scattering with mean bond lengths and the values obtained from structure refinement was obtained by ordering most of the Mn²⁺ to the *M*(4) site.

Although metamorphic amphiboles are normally low in Mn (< 0.20 apfu), reflecting their Mn-poor protoliths (Schumacher, 2007), there are many reports of amphibole finds classified as clino-ferro-suenoite globally (<http://www.mindat.org>, last access: 19 March 2025). Unsurprisingly, the more Mn-rich varieties are from Mn-silicate skarns (with rhodonite, spessartine, etc.) with compositions on the join formed with clino-suenoite (e.g., Yoshimura and Momoi, 1961; Nambu et al., 1980; Melcher, 1995; Mancini et al., 2000; Myslan et al., 2023). Pure end-member □Mn₂Fe₅²⁺Si₈O₂₂(OH)₂ has not been reported so far; possibly the closest found is a sample from Broken Hill, Australia, with nominally ^BMn = 1.49 and ^CFe²⁺ = 3.86 apfu (Mason, 1973). The most ^BMn-rich varieties found, up to 1.65 apfu (Vassileva and Bonev, 2001) and 1.86–1.87 apfu (Mücke, 2005; Myslan et al., 2023), are often also rich in Mg and thus straddling the clino-suenoite compositional field, suggesting that the incorporation of Mn at *M*(4) is facilitated by higher Mg contents at the *C* positions. To the best of our knowledge, there is no evidence from synthesis experiments to validate the stability of the monoclinic end-member. In fact, the ^BMn-dominant amphiboles with the highest fraction of ^CFe²⁺ known in nature are shown to be orthorhombic, with space group symmetry *Pnmm* (Sueno et al., 2002), and thus recognized under the name proto-ferro-suenoite (Williams et al., 2013).

Based on the textural relations observed, clino-ferro-suenoite at Hilläng likely formed by partial replacement of olivine in reactions with a metamorphic Si-rich fluid during retrograde conditions according to the (idealized) reaction (Fe_{1.43}Mn_{0.57})SiO₄ + 9 SiO₂(aq) + 2 H₂O = 2 Mn₂Fe₅²⁺Si₈O₂₂(OH)₂. Alteration of manganian fayalite into Mn-bearing grunerite accompanied by magnetite precipitation was previously reported by Janeczek (1989), invoking a post-magmatic hydrothermal process rather than formation during retrograde metamorphism. Normally, monoclinic amphiboles show strongly negative to neutral Eu anomalies

(e.g., Skublov and Drugova, 2003; Holtstam et al., 2014; Bernard et al., 2020); the present exotic feature may be inherited from the olivine precursor.

Finally, it may be noted that Weibull (1883) described an Mn-bearing amphibole named “silfbergite”, from Väster Silfberg (Stollberg ore field), 6 km NE from Hilläng. It has been considered a synonym of “dannemorite” (Leake, 1978). We have analysed such a “silfbergite” sample (GEO-NRM no. 19530359); this one was shown to be a manganoan grunerite.

Data availability. A CIF is deposited in the Supplement.

Supplement. The supplement related to this article is available online at <https://doi.org/10.5194/ejm-37-221-2025-supplement>.

Author contributions. Conceptualization: DH; data collection and interpretation: all authors; manuscript writing: DH and FC with contributions from all co-authors.

Competing interests. The contact author has declared that none of the authors has any competing interests.

Disclaimer. Publisher’s note: Copernicus Publications remains neutral with regard to jurisdictional claims made in the text, published maps, institutional affiliations, or any other geographical representation in this paper. While Copernicus Publications makes every effort to include appropriate place names, the final responsibility lies with the authors.

Special issue statement. This article is part of the special issue “Celebrating the outstanding contribution of Paola Bonazzi to mineralogy”. It is not associated with a conference.

Acknowledgements. It is a privilege for us to contribute to this special issue of the *European Journal of Mineralogy* in honour of eminent crystallographer Paola Bonazzi and her long-standing dedicated work. Her death is a huge loss for the mineralogical community in Europe. We thank Matteo Alvaro (University of Pavia) for access to the Laboratorio di Mineralogia Sperimentale “Fiorenzo Mazzi”. We also thank Roberta Oberti and an anonymous referee for useful constructive reviews.

Financial support. Fernando Cámara was supported by the Italian Ministry of University (MIUR) through the project “Dipartimenti di Eccellenza 2023-2027”.

The publication of this article was funded by the Swedish Research Council, Forte, Formas, and Vinnova.

Review statement. This paper was edited by Dmitry Pushcharovsky and reviewed by Roberta Oberti and one anonymous referee.

References

- Apopei, A. I., Buzgar, N., and Buzatu, A.: Raman and infrared spectroscopy of kaersutite and certain common amphiboles. *Analele Stiintifice ale Universitatii “Al I Cuza” din Iasi Seria Geologie*, 57, 35–58, 2011.
- Beetsma, J. J.: Retrograde fluid evolution of the Stollberg Pb–Zn–Fe–Mn(Ag) ore deposit, central Bergslagen, Sweden. *Geol. Fören. Stock. Förhandl.*, 114, 279–290, 1992.
- Bernard, C., Estrade, G., Salvi, S., Béziat, D., and Smith, M.: Alkali pyroxenes and amphiboles: a window on rare earth elements and other high field strength elements behavior through the magmatic-hydrothermal transition of peralkaline granitic systems. *Contrib. Mineral. Petrol.*, 175, 1–27, <https://doi.org/10.1007/s00410-020-01723-y>, 2020.
- Boffa Ballaran, T., McCammon, C. A., and Carpenter, M. A.: Order parameter behavior at the structural phase transition in cumingtonite from Mössbauer spectroscopy. *Am. Mineral.*, 87, 1490–1493, 2002.
- Cipriani, C.: Amphiboles: historical perspective. *Rev. Mineral. Geochem.*, 67, 517–546, 2007.
- Clark, A. M.: Hey’s mineral index: mineral species, varieties and synonyms, Chapman and Hall, London, 852 pp., ISBN 0412399504, 1993.
- Dana, J. D.: Fourth supplement to Dana’s mineralogy. *Am. J. Sci. Arts*, 24, 107–132, 1857.
- Erdmann, A.: Dannemora jernmalmsfält i Upsala län, till dess geognostiska beskaffenhet skildradt; Ett försök af Axel Erdmann, Kongliga Vetenskaps-Akademiens Handlingar för år 1850, 1–138, 1851 (in Swedish).
- Finger, L. W.: The crystal structure and cation distribution of a grunerite. *Mineralogical Society of America Special Paper*, 2, 95–100, 1969.
- Geijer, P. and Magnusson, N. H.: De mellansvenska järnmalmenas geologi. Norstedt, 654 pp., ISSN 0348-1352, 1944 (in Swedish).
- Goldman, D. S.: A reevaluation of the Mössbauer spectroscopy of calcic amphiboles. *Am. Mineral.*, 64, 109–118, 1979.
- Greenwood, N. N. and Gibb, T. C.: Mössbauer spectroscopy, Chapman and Hall. 658 pp., <https://doi.org/10.1007/978-94-009-5697-1>, Softcover ISBN 978-94-009-5699-5, 1971.
- Haüy, R. J.: *Traité de minéralogie*, Vol 1, Chez Louis, Paris, 494 pp., 1801 (in French).
- Hawthorne, F. C. and Della Ventura, G.: Short-range order in amphiboles. in: *Amphiboles: Crystal chemistry, occurrence and health issues*, edited by: Hawthorne, F. C., Oberti, R., Della Ventura, G., and Mottana, A., *Rev. Mineral. Geochem.*, 67, 173–222, 2007.
- Hawthorne, F. C. and Oberti, R.: Amphiboles: Crystal Chemistry. in: *Amphiboles: Crystal chemistry, occurrence and health issues*, edited by: Hawthorne, F. C., Oberti, R., Della Ventura, G., and Mottana, A., *Rev. Mineral. Geochem.*, 67, 125–172, 2007.
- Hawthorne, F. C., Oberti, R., Harlow, G. E., Maresch, W. V., Martin, R. F., Schumacher, J. C., and Welch, M. D.: Nomenclature of the amphibole supergroup. *Am. Mineral.*, 97, 2031–2048, <https://doi.org/10.2138/am.2012.4276>, 2012.

- Hirschmann, M., Evans, B. W., and Yang, H.: Composition and temperature dependence of Fe-Mg ordering in cummingtonite-grunerite as determined by X-ray diffraction, *Am. Mineral.*, 79, 862–877, 1994.
- Holland, T. J. B. and Redfern, S. A. T.: Unit cell refinement from powder diffraction data: the use of regression diagnostics, *Mineral. Mag.*, 61, 65–77, 1997.
- Holtstam, D., Andersson, U. B., Broman, C., and Mansfeld, J.: Origin of REE mineralization in the Bastnäs-type Fe-REE-(Cu-Mo-Bi-Au) deposits, Bergslagen, Sweden, *Miner. Deposita*, 49, 933–966, <https://doi.org/10.1007/s00126-014-0553-0>, 2014.
- Igelström, L. J.: Hillängsite, nouveau minéral de la mine de fer de Hilläng, paroisse Ludvika, gouvernement de Dalarna (Suède), *Bull. Minéral.*, 76, 232–234, 1884 (in French).
- Janczek, J.: Manganooan fayalite and products of its alteration from the Strzegom pegmatites, Poland, *Mineral. Mag.*, 53, 315–325, 1989.
- Jansson, N. F., Erismann, F., Lundstam, E., and Allen, R. L.: Evolution of the Paleoproterozoic volcanic-limestone-hydrothermal sediment succession and Zn–Pb–Ag and Fe-oxide deposits at Stollberg, Bergslagen, Sweden, *Econ. Geol.*, 108, 309–335, <https://doi.org/10.2113/econgeo.108.2.309>, 2013.
- Jochum, K. P., Willbold, M., Raczek, I., Stoll, B., and Herwig, K.: Chemical Characterisation of the USGS Reference Glasses GSA-1G, GSC-1G, GSD-1G, GSE-1G, BCR-2G, BHVO-2G and BIR-1G Using EPMA, ID-TIMS, ID-ICP-MS and LA-ICP-MS, *Geostand. Geoanalytical Res.*, 29, 285–302, <https://doi.org/10.1111/j.1751-908X.2005.tb00901.x>, 2005.
- Kenngott, G. A.: Dannemorit (ein neuer Amphibol-Spath), Übersicht der Resultate mineralogischer Forschungen in den Jahren 1856 und 1857, edited by: Engelmann, W., 1856 (in German).
- Leake, B. E.: Nomenclature of amphiboles, *Am. Mineral.*, 63, 1023–1052, 1978.
- Leake, B. E., Woolley, A. R., Arps, C. E., Birch, W. D., Gilbert, M. C., Grice, J. D., Hawthorne, F. C., Kato, A., Kisch, H. J., Krivovichev, V. G., Linthout, K., Laird, J., Mandarino, J. A., Maresch, W. V., Nickel, E. H., Rock, N. M. S., Schumacher, J. C., Smith, D. C., Stephenson, N. C. N., Ungaretti, L., Whittaker, E. J. W., and Guo, Y.: Nomenclature of amphiboles; report of the Subcommittee on Amphiboles of the International Mineralogical Association Commission on new minerals and mineral names, *Mineral. Mag.*, 61, 295–310, 1997.
- Leißner, L.: Crystal chemistry of amphiboles studied by Raman spectroscopy, MSc thesis, Mineralogisch-Petrographisches Institut-Universität Hamburg, Hamburg, Germany, 45 pp., <https://www.geo.uni-hamburg.de/mineralogie/masterarbeiten/leissner-msc-thesis.pdf> (last access: 19 November 2024), 2014.
- Mancini, F., Alviola, R., Marshall, B., Satoh, H., and Papunen, H.: The manganese silicate rocks of the early Proterozoic Vittinki Group, southwestern Finland: Metamorphic grade and genetic interpretations, *Can. Mineral.*, 38, 1103–1124, <https://doi.org/10.2113/gscanmin.38.5.1103>, 2000.
- Mandarino, J. A.: The Gladstone-Dale compatibility of minerals and its use in selecting mineral species for further study, *Can. Mineral.*, 45, 1307–1324, 2007.
- Mason, B.: Manganese silicate minerals from Broken hill, New South Wales, *Aust. J. Earth Sci.*, 20, 397–404, 1973.
- Melcher, F.: Genesis of chemical sediments in Birimian greenstone belts: evidence from gondites and related manganese-bearing rocks from northern Ghana, *Mineral. Mag.*, 59, 229–251, 1995.
- Merli, M., Ungaretti, L., and Oberti, R.: Leverage analysis and structure refinement of minerals, *Am. Mineral.*, 85, 532–542, 2000.
- Mücke, A.: The Nigerian manganese-rich iron-formations and their host rocks – from sedimentation to metamorphism, *J. Afr. Earth Sci.*, 41, 407–436, <https://doi.org/10.1016/j.jafrearsci.2005.07.003>, 2005.
- Myslan, P., Stevko, M., and Mikus, T.: Mineralogy and genetic aspects of the metamorphosed manganese mineralization at the Julius ore occurrence near Betliar (Gemeric Unit, Western Carpathians, Slovakia), *J. Geosci.*, 68, 313–332, <https://doi.org/10.3190/jgeosci.384>, 2023.
- Nambu, M., Tanida, K., and Kitamura, T.: Chemical composition of manganese-bearing amphibole from Japan and its classification, *Mineral. J.*, 14, 98–116, 1980 (in Japanese).
- Oberti, R., Hawthorne, F. C., and Raudsepp, M.: The behaviour of Mn in amphiboles: Mn in synthetic fluor-edenite and synthetic fluor-pargasite, *Eur. J. Mineral.*, 9, 115–122, 1997.
- Oberti, R., Hawthorne, F. C., Cannillo, E., and Cámara, F.: Long-range order in amphiboles, in: *Amphiboles: Crystal chemistry, occurrence and health issues*, edited by: Hawthorne, F. C., Oberti, R., Della Ventura, G., and Mottana, A., *Rev. Mineral. Geochem.*, 67, 125–172, 2007.
- Oberti, R., Boiocchi, M., Hawthorne, F. C., Ciriotti, M. E., Revheim, O., and Bracco, R.: Clino-suenoite, a newly approved magnesium-iron-manganese amphibole from Valmalenco, Sondrio, Italy, *Mineral. Mag.*, 82, 189–198, <https://doi.org/10.1180/minmag.2017.081.034>, 2018.
- Ohlsson, L. G.: Prospekteringsrapport GRB 078, *Geologiska kartbladet 12F Ludvika 4d*, Geological Survey of Sweden, 13 pp., 1979 (in Swedish).
- Prescher, C., McCammon, C., and Dubrovinsky, L.: MossA: a program for analyzing energy-domain Mössbauer spectra from conventional and synchrotron sources, *J. Appl. Cryst.*, 45, 329–331, <https://doi.org/10.1107/S0021889812004979>, 2012.
- Ripa, M.: The mineral chemistry of hydrothermally altered and metamorphosed wall-rocks at the Stollberg Fe-Pb-Zn-Mn (-Ag) deposit, Bergslagen, Sweden, *Miner. Deposita*, 29, 180–188, 1994.
- Robinson, K., Gibbs, G. V., and Ribbe, P. H.: Quadratic elongation: a quantitative measure of distortion in coordination polyhedra, *Science*, 172, 567–570, 1971.
- Schumacher, J. C.: Metamorphic amphiboles: composition and co-existence, in: *Amphiboles: Crystal chemistry, occurrence and health issues*, edited by: Hawthorne, F. C., Oberti, R., Della Ventura, G., and Mottana, A., *Rev. Mineral. Geochem.*, 67, 359–416, 2007.
- Skublov, S. and Drugova, G.: Patterns of trace-element distribution in calcic amphiboles as a function of metamorphic grade, *Can. Mineral.*, 41, 383–392, 2003.
- Shannon, R. D.: Revised effective ionic radii and systematic studies of interatomic distances in halides and chalcogenides, *Acta Cryst. A*, 32, 751–767, 1976.
- Sheldrick, G. M.: Crystal Structure Refinement with SHELXL, *Acta Cryst.*, C71, 3–8, 2015.

- Sueno, S., Matsuura, S., Bunno, M., and Kurosawa, M.: Occurrence and crystal chemical features of protoferro-anthophyllite and protomangano-ferro-anthophyllite from Cheyenne Canyon and Cheyenne Mountain, USA and Hirukawa-mura, Suisho-yama, and Yokone-yama, Japan, *J. Miner. Petrol. Sci.*, 97, 127–136, <https://doi.org/10.2465/jmps.97.127>, 2002.
- Vassileva, R. D. and Bonev, I. K.: Manganoan amphiboles from the skarn-ore Pb-Zn deposits in the Madan District, Central Rhodopes, Bulgaria, Bulgarian Academy of Science, Geochemistry, *Miner. Petrol.*, 38, 45–53, 2001.
- Weibull, M.: Några manganmineral från Vester-Silfberget i Dalarne, *Geol. Fören. Stock. Förhandl.*, 6, 499–509, <https://doi.org/10.1080/11035898309444094>, 1883 (in Swedish).
- Williams, P., Hatert, F., Pasero, M., and Mills, S.: IMA Commission on New Minerals, Nomenclature and Classification (CNMNC), Newsletter 16. New minerals and nomenclature modifications approved in 2013, *Mineral. Mag.*, 77, 2695–2709, 2013.
- Wilson, S. A.: G-probe 20 summary report: International Association of Geoanalysts G-probe 20 Report, <https://www.geoanalyst.org/wp-content/uploads/2021/02/GP-20-report.pdf> (last access: 19 November 2024), 2018.
- Wu, S., Wörner, G., Jochum, K.P., Stoll, B., Simon, K., and Kronz, A.: The preparation and preliminary characterisation of three synthetic andesite reference glass materials (ARM-1, ARM-2, ARM-3) for in situ microanalysis, *Geostand. Geoanalytical Res.*, 43, 567–584, <https://doi.org/10.1111/ggr.12301>, 2019.
- Yang, H., Hazen, R. M., Prewitt, C. T., Finger, L. W., Lu, R., and Hemley, R. J.: High-pressure single-crystal X-ray diffraction and infrared spectroscopic studies of the *C2/m-P21/m* phase transition in cummingtonite, *Am. Mineral.*, 83, 288–299, 1998.
- Yong, T., Dera, P., and Zhang, D.: Single-crystal X-ray diffraction of grunerite up to 25.6 GPa: a new high-pressure clinoamphibole polymorph, *Phys. Chem. Miner.*, 46, 215–227, <https://doi.org/10.1007/s00269-018-0999-1>, 2019.
- Yoshimura, T. and Momoi, H.: Dannemorite from Zomeki, Yamaguchi Prefecture. The science reports of the Faculty of Science, Kyushu University, *Geology*, 5, 99–110, 1961 (in Japanese).
- Zhang, L. and Hafner, S. S.: Gamma resonance of ^{57}Fe in grunerite at high pressures, *Am. Mineral.*, 77, 474–479, 1992.